RSC Advances

PAPER

View Article Online
View Journal | View Issue

Cite this: *RSC Adv.*, 2020, **10**, 7559

The effect of size and surface ligands of iron oxide nanoparticles on blood compatibility†

Tao Liu,‡[ab] Ru Bai,‡[a] Huige Zhou,‡[a] Rongqi Wang,[c] Jing Liu,[ad] Yuliang Zhao[ab] and Chunying Chen*[ab]

Superparamagnetic iron oxide nanoparticles (SPIONs) have been widely used and have attracted increased attention for their unique physicochemical properties, especially in biomedical sciences as contrast agents following intravenous administration. However, only few studies have systematically reported the blood compatibility of iron oxide nanoparticles with different physicochemical properties such as different sizes and surface ligands. Therefore, we selected three widely used organic ligands (polyacrylic acid, hyaluronic acid, and chitosan) with modified SPIONs at the same size of 5–6 nm, and polyacrylic acid-modified SPIONs with different sizes (5, 10, and 30 nm) at different concentrations to evaluate their haemocompatibility. Our results revealed that SPIONs modified with polyacrylic acid demonstrated size-dependent destruction of red blood cells and complement activation. Interestingly, 5 nm SPIONs prolonged blood clotting time as compared with 10 nm and 30 nm SPIONs *in vitro*. Compared with polyacrylic acid-modified SPIONs, hyaluronic acid- and chitosan-modified SPIONs least affected red blood cells, platelets, coagulation, and complement activation. Hence, hyaluronic acid- and chitosan-coated SPIONs are more suitable for nanomedicine applications than polyacrylic acid-coated SPIONs. Furthermore, the interaction between SPIONs and blood components strongly correlated with the administered concentration of nanoparticles. These results will provide some experimental information for safe-by-design SPIONs.

Received 27th December 2019
Accepted 11th February 2020

DOI: 10.1039/c9ra10969b

rsc.li/rsc-advances

Introduction

Superparamagnetic iron oxide nanoparticles (SPIONs) play an important role in biomedicine due to their characteristics of simple preparation, uniform size distribution, good biocompatibility[1] and the possibility of functional surfaces[2–4] for applications such as tumour or vascular imaging, drug delivery, gene therapy, hyperthermia, *in vitro* tracking of labelled cells, magnetic separation of cells or molecules and iron supplementation in anaemia patients.[5–7] Recent research found that iron oxide nanoparticles are capable of activating toll-like receptor-4 signalling and interacting with macrophages to regulate the immune system.[8] SPIONs also have been approved by the FDA for use in clinic applications several years ago. However, some SPIONS have been withdrawn from the market because of side effects. For example, Feridex® could not be administered as an intravenous bolus because of possible severe backache, and Resovist® has been shown incapable of differentiating hepatocellular carcinoma from healthy liver tissue.[9] It is imperative to evaluate the biosafety of nanoparticles before their widespread use in the market.

Most biomedical applications of SPIONs utilise intravenous (i.v.) administration, which would expose to the blood first. Research showed that nanoparticles possess a risk of haemolysis, platelet aggregation, or blood coagulation.[10] According to ISO-10993-4,[11] the safety evaluation of medical devices should contain red blood cells, platelets, and the coagulation and complement system. Haemolysis is defined as the loss of erythrocyte membrane integrity, inducing haemoglobin release into the surroundings, which can lead to anaemia, jaundice, and other pathological symptoms.[12] Platelets, the central mediators of thrombotic events, aggregate because of biomaterials related to thrombosis and coagulation.[13] Unbalance of

[a]*CAS Key Laboratory for Biomedical Effects of Nanomaterials and Nanosafety, CAS Center for Excellence in Nanoscience, National Center for Nanoscience and Technology, Beijing 100190, P. R. China. E-mail: chenchy@nanoctr.cn; Fax: +86-10-62656765; Tel: +86 10 8254 5560*

[b]*University of Chinese Academy of Sciences, Beijing 100049, P. R. China*

[c]*Department of Clinical Laboratory, Beijing Haidian Hospital, Haidian Section of Peking University Third Hospital, Beijing 100080, P. R. China*

[d]*Faculty of Life Sciences & Medicine, Northwest University (NWU), Xi'an 710069, P. R. China*

† Electronic supplementary information (ESI) available: Zeta potential distribution of SPIONs, size characterisation of Feraheme, characterisations of FTIR spectrum and magnetic property of SPIONs, T_1 and T_2 weighted MRI images of SPIONs at different concentrations of iron, plots of R_1 and R_2 *versus* Fe concentration of SPIONs, picture of SPIONs and the hydrodynamic size of SPIONs in PBS solution at different time points, and results of four coagulation tests after addition of healthy plasma into the abnormal plasma treated by Fe_3O_4@5PAA at the concentration of 5 mg mL^{-1}. See DOI: 10.1039/c9ra10969b

‡ Tao Liu, Ru Bai and Huige Zhou contributed equally to this work.

anticoagulation and pro-coagulation is caused by the activation of the coagulation system, which may bring about life-threatening toxicities.[14] The complement system is a critical component of innate immunity, which is in charge of recognising, eliminating, and destroying pathogens.[15] Therefore, the blood contact properties of SPIONs should always be evaluated carefully and systematically prior to clinical utilisation.

Several studies have researched the effect of different super paramagnetic iron oxide nanoparticles on blood with different measurement methods and conditions. Soundararajan *et al.* reported that curcumin-SPION (γ-Fe_2O_3, 45.26 $\pm$ 5.36 nm) integrated poly (lactic acid) (PLA) nanofibers activated platelets and deformed RBC membrane integrity.[16] Nemmar *et al.* found that ultra-small super paramagnetic iron oxide nanoparticles (magnetite, Fe_3O_4, 4–6 nm) caused thrombosis and cardiac oxidative stress and DNA damage in mice following acute intravenous administration.[17] Li's group[18] reported that Fe_3O_4 magnetic nanoparticles (72.6 $\pm$ 0.57 nm) cause eryptosis, and changes in flow properties of blood. Moreover, some researchers evaluated the haematotoxicity of magnetic nanoparticles coated with dimercaptosuccinic acid (DMSA) and polyethylene glycol (PEG) *in vitro* and *in vivo* in a rat model.[19] *In vitro* analyses revealed prolonged APTT (activated partial thromboplastin time) values for DMSA compared with PEG-coated nanoparticles. There was a significant effect on the leukocyte counts in animals treated with DMSA-coated nanoparticles compared with the PEG-modified group. Biological effects and toxicity of SPIONs are complicated because of their diverse physical–chemical properties and the experimental methods such as incubation time, the wavelength at which haemoglobin is quantified, and the blood source (human or rabbit).

Different surface ligands[20] and different sizes[21] will render unique physicochemical properties of SPIONs, which allow for a broad range of applications such as magnetic resonance imaging, drug targeting, among others. Hyaluronic acid (HA) possesses[22,23] enzymatic degradation properties and specifically binds to cancer cells overexpressing CD44.[24,25] Our previous work indicated that SPIONs coated with HA could target tumour cells and tune the T_1- and T_2-weighted MRI by aggregating in the tumour microenvironment.[26] Chitosan (CS), derived from chitin, is a biocompatible and biodegradable linear polysaccharide with antimicrobial properties and affinity for many molecules.[27] Polyacrylic acid (PAA), an aqueous soluble polymer, has been widely used as a surface coating, which is considered as safe modification.[28] For Fe_3O_4@10PAA and Fe_3O_4@30PAA can be conveniently obtained, this study specifically investigated the effect of different sizes (5, 10, 30 nm) and surface ligands (HA, CS, PAA) on the haematological parameters of SPIONs *in vitro* and *in vivo.* To provide a systematic overview of the blood biocompatibility of SPIONs, Feraheme, a kind of iron oxide nanoparticles approved by the FDA, was chosen as the standard material and some dosages of its preclinical evaluations were chosen as the reference. We carefully investigated the morphology and lysis of red blood cells (RBCs), platelet activation, coagulation, complement activation, and effects of vascular endothelial cells after treatment with five kinds of SPIONs *in vivo* and *in vitro*. We found that HA- and CS-modified SPIONs were safer than PAA-modified SPIONs, and the effect of SPIONs on blood compatibility showed strong size dependence.

Experimental

Materials

All solvents and reagents were purchased from Beijing Chemical Works and used without further purification unless stated otherwise. Polyacrylic acid (PAA) was purchased from Acros Organics. Hyaluronic acid (HA, M_w = 6.8 kDa) was obtained from Shandong Freda Biopharmaceutical Co., Ltd (Shandong, China). Low-molecular-weight chitosan (CS) was purchased from Sigma-Aldrich. Fe_3O_4@10PAA and Fe_3O_4@30PAA were obtained from Xi'an Ruixi Biological Technology Co., Ltd (Shanxi, China). Feraheme, a clinical iron supplementation agent, was purchased from AMAG (Waltham, USA). Dulbecco's modified Eagle's medium (DMEM), penicillin–streptomycin (PS), and fetal bovine serum (FBS) were bought from WISENT Inc (Quebec, Canada). Female BALB/c mice were purchased from Beijing Vital River Experimental Animal Technology Co. Ltd. (Beijing, China). All experiments were performed in compliance with the relevant laws and followed institutional guidelines of National Centre for Nanoscience and Technology of China. All animal experiments were also approved by the relevant institutional committee of National Centre for Nanoscience and Technology of China.

The culture conditions for HUVEC cells were DMEM supplemented with 10% FBS and 1% PS at 37 °C in a humidified atmosphere of 5% CO_2. In this work, all mice were housed in a sterile animal room (temperature 22 $\pm$ 2 °C, with a 12 h light/dark cycle).

Human blood sample

All human blood samples were from healthy volunteers and the related studies were approved by the Medical Ethics Committee of Beijing Haidian Hospital. All procedures were conducted in accordance with the approved guidelines of Beijing Haidian Hospital. The authors declare that informed consent was obtained from all human subjects.

Preparation of SPIONs

Hyaluronic acid-modified iron oxide nanoparticle (Fe_3O_4@HA) was synthesised by a modified high-temperature co-precipitation method.[26] Briefly, 0.50 g HA was dissolved in 50 mL distilled water, and the solution was heated to 102 °C in an oil bath. Oxygen in the system was removed for 30 min under a nitrogen gas atmosphere. Meanwhile, $FeCl_3 \cdot 6H_2O$ (0.54 mmol) and $FeCl_2 \cdot 4H_2O$ (0.36 mmol) were precisely weighed and dissolved in dilute HCl solution (2 mL, 1.0 M). The prepared iron ion solution was quickly injected into the solution under a nitrogen atmosphere with constant and vigorous stirring. A total of 15 mL ammonia solution was added dropwise to adjust the pH value of the reaction solution to 9–10. The reaction mixture was refluxed for 40 min, then cooled to room

temperature and dialyzed for 3 days in a dialysis bag (MWCO 12000–14000 Da) to remove unreacted reagents. After dialysis, SPIONs were filtered through a 0.22 μm filter membrane and saved in a glass bottle. Polyacrylic acid modified iron oxide nanoparticle (Fe_3O_4@5PAA) was synthesised in the same process. Chitosan-modified iron oxide nanoparticle (Fe_3O_4@CS) was also synthesised in the same way, except the pH value of the reaction solution was 6.9.

Characterisation of SPIONs

The size and morphology were visualised using a FEI Tecnai G2-20S-TWIN electron microscope (Hillsboro, USA). The hydrodynamic size and zeta potential of materials were measured with a Zeta Sizer Nano series Nano-ZS (Malvern Instruments Ltd, Malvern, UK). The super paramagnetic properties of iron oxide nanoparticles were analyzed using PPMS-9 (Quantum Design Inc, San Diego, USA). The Fe elemental content was measured using ICP-OES (PE8000, PerkinElmer, Waltham, USA). FTIR spectra of nanoparticles were collected with a Fourier transform infrared spectrometer (Spectrum One, PerkinElmer, Waltham, USA).

Relaxivity measurement

The relaxation measurements were performed using a 7.0 T small-animal MRI instrument (BioSpec 7.0 70/20 USR, Bruker, Karlsruhe, Germany). A series of aqueous solutions of SPIONs with different iron concentrations were aliquoted to 0.5 mL tubes. The T_1_rapid acquisition relaxation enhancement (T_1_RARE) sequence was used to obtain T_1-weighted images and the parameters were as follows: TR = 300 ms, TE = 6.06 ms, field of view = 35 × 35 mm, matrix size = 256 × 256, number of slices = 10, slice thickness = 1 mm, flip angle = 90°, NEX = 4.0. The T_2_Turbo RARE sequence was used to obtain T_2-weighted images and the parameters were as follows: TR = 3000 ms, TE = 50 ms, field of view = 35 × 35 mm, matrix size = 256 × 256, number of slices = 10, slice thickness = 1 mm, flip angle = 90°, NEX = 1.0.

Effect of SPIONs on RBC morphology and lysis

RBC lysis. RBC lysis was evaluated with the modified ASTM standard E 2524-08.[29] Haemoglobin standards were prepared using a haemoglobin standard and cyan methaemoglobin (CMH) reagent to construct a standard curve at the range of haemoglobin concentration from 0.025 to 0.8 mg mL^{-1}. Fresh anticoagulated whole blood was collected from a healthy rabbit and centrifuged at 1000 × *g* for 15 min to get supernatant plasma. Then 200 μL of each calibration standard and blank (CMH reagent) were added to each well of a 96-well plate. Thereafter, 200 μL of the total blood haemoglobin (TBH) sample was prepared by mixing 20 μL of the pooled whole blood, 5.0 mL of CMH reagent, and 100 μL of plasma (PFH) were added per well of the 96-well plate. A total of 100 μL of CMH reagent was added to the well containing the plasma. The plate was sealed and gently shaken on a plate shaker for 1–2 min. The absorbance at 540 nm was measured to determine haemoglobin concentration.

Moreover, the plasma-free haemoglobin (PFH) should be below 1 mg mL^{-1}, otherwise the blood was unqualified and need to be collected again. Next, pooled whole blood was diluted with Ca^{2+}/Mg^{2+}-free PBS (DPBS) to adjust the TBH concentration to 10 ± 1 mg mL^{-1} (TBHd). Next, different concentrations of SPIONs were diluted with DPBS and diluted whole blood then incubated at 37 °C for 3 h after mixture. A 40% PEG and a 10% Triton X-100 solution were used as a negative and positive control, respectively. These mixtures were centrifuged for 15 min at 1000 × *g* and the supernatant was collected. The haemoglobin concentration of the supernatant was measured following the above method.

RBC morphology. The impact of SPIONs on RBC morphology RBCs were evaluated using SEM. The procedures are as follows: fresh citrate-anticoagulated rabbit whole blood was centrifuged at 1000 × *g* for 10 min, and the supernatant was carefully removed. The RBC pellet was washed with PBS three times until the supernatant was colourless. Then a 2% RBC suspension was prepared by diluting the RBC pellet with PBS, which was incubated for 2 h at 37 °C with different concentrations of the SPIONs, then dissolved in PBS. Subsequently, 50 μL of RBCs were deposited on glass slides and fixed with 2.5% glutaraldehyde overnight. The fixed RBCs were washed with PBS twice and dehydrated with 60%, 70%, 80%, 90%, and 100% (v/v) ethanol for 10 min, respectively, and dried in air. The dried RBCs were coated with gold and observed with a scanning electron microscope (SEM, S4800). Finally, 5000× magnification fields of view representing the entire RBC morphology were selected.

Complement activation by SPIONs

A human C3a ELISA kit (BD, USA) was used to measure the expression of the activation peptide (C3a) to evaluate complement activation by SPIONs. Briefly, fresh anticoagulated whole blood from healthy volunteers was centrifuged at 1000 × *g* for 15 minutes, and platelet-poor plasma was collected and diluted with PBS. The volume ratio of plasma to PBS was 3 : 1. Then different concentrations of SPIONs were mixed at a volume ratio of 1 : 4 with the plasma and incubated at 37 °C for 30 min. After that, the mixture was diluted (300×) with a standard diluent provided in the kit. A total of 50 μL of ELISA diluent was added to each well of a 96-well plate pre-coated with an anti-human C3a antibody. Then, 100 μL of the standard and the diluted samples were pipetted into appropriate wells and incubated for 2 h at 25 °C. Wells were washed five times with 300 μL per well of the prepared wash buffer after the supernatant was discarded. The prepared detection antibody was added to each well, which was covered with a plate sealer and incubated for 1 hour at room temperature. A total of 100 μL of TMB one-step reagent was added to each well after washing seven times. The plate was incubated for 30 minutes at room temperature in the dark. Then 50 μL of stop solution was added to each well, and the absorbance of the solution was measured at 450 nm within 30 minutes of stopping the reaction.

The effect of SPIONs on *in vitro* and *in vivo* blood coagulation

The effect of SPIONs on blood coagulation was evaluated *in vitro* through four coagulation indices. Briefly, platelet-poor plasma (PPP) was prepared by centrifuging fresh citrate-anticoagulated

blood samples at 1000 × *g* for 15 min. The PPP was added to the SPIONs at different concentrations at a ratio of 9 : 1, and the final nanoparticle concentrations were 500, 100, 20, and 4 μg mL^{-1}. After incubation for 30 min at 37 °C, the supernatant plasma was collected to measure APTT (activated partial thromboplastin time), PT (prothrombin time), TT (thrombin time), and FIB (fibrinogen) with an automatic coagulation analyzer (ACT TOP 700, Werfen, Spain). The same volume of PBS with SPION samples was used as a negative control.

The effect of SPIONs on blood coagulation was also evaluated *in vivo* with the same method as *in vitro*. Briefly, eighty-two female BALB/c mice (body weight: 18–20 g) were randomly divided into seven groups. Five SPIONs, Feraheme, and PBS were intravenously injected into every group at a dose of 20 mg kg^{-1} body weight. Six mice of each group were sacrificed at the time points of 30 min and 24 h post-administration, and anticoagulation blood samples were collected. Then the plasma was separated by centrifugation for the four coagulation tests as previously described.

Platelet activation by SPIONs

Fresh citrate-anticoagulated whole blood from healthy human volunteers was centrifuged at 100×*g* for 5 min, and the platelet-rich plasma (PRP) from the supernatant was collected. Then 100 μL of PRP was mixed thoroughly with 25 μL of SPIONs. The mixture was incubated for 15 min at 37 °C. Finally, the number of platelets was counted using a blood cell analyzer. A total of 1 mg mL^{-1} of collagen and DPBS were used as positive and negative controls. The platelet aggregation rate was calculated as follows: the percent platelet aggregation (PA%) = (platelet count in the negative group − the platelet count in the sample group)/the platelet count in the negative group × 100%. Results were considered positive when the rate exceeded 20%.

Cytotoxicity of SPIONs in human umbilical vein endothelial cells

Human umbilical vein endothelial cells (HUVEC cell line) were selected to evaluate the vascular endothelial cytotoxicity of SPIONs. HUVECs were seeded in 96-well plates at a density of approximately 4000 cells per well. After 12 hours, the medium was replaced by fresh medium containing SPIONs (25, 50, 100, 200, 400 μg mL^{-1}, in terms of Fe element). The cells were incubated for 24 hours. Finally, the wells were washed with PBS twice after the medium was discarded, and a 100 μL mixture of CCK-8 reagent and the medium (1 : 10) was added into the wells. The absorbance values were measured at 450 nm (with a reference wavelength of 650 nm).

Statistical analysis

The data were represented as the mean ± SD (standard deviation) and statistically analyzed using SPSS. The difference was considered significant when $p < 0.05$ (*), $p < 0.01$ (**), and $p < 0.001$ (***).

Results and discussion

Physicochemical characterisation of SPIONs

Three types of SPIONs modified by PAA, HA, and CS were synthesised using a high temperature co precipitation method. We have used Fe_3O_4 particles with a surface ligands and different sizes and named them as Fe_3O_4@5PAA, Fe_3O_4@10PAA and Fe_3O_4@30PAA, and the other two were named as Fe_3O_4@HA and Fe_3O_4@CS. TEM results showed that the mean size of three synthesised nanoparticles was 5–6 nm, and the sizes of the two purchased PAA-modified SPIONs were about 10 nm and 30 nm, respectively (Fig. 1A and B), and that they were dispersed uniformly. The hydrodynamic size of each particle showed that SPIONs with different surface ligands had similar sizes, approximately 30 nm each, while the hydrodynamic diameter of Fe_3O_4@10PAA and Fe_3O_4@30PAA were about 40 nm and 60 nm, respectively (Fig. 1C). In the FTIR spectra of the SPIONs (Fig. S2A†), the Fe_3O_4@*n*PAA display similar peaks and the peak at approximately 1710 cm^{-1} was ascribed to a C=O stretching vibration of PAA. The 1072 cm^{-1} peak is the characteristic peak of HA (C–N bonds stretching vibration), indicating the presence of HA on the surface of Fe_3O_4. The signature peak of Fe_3O_4@CS was found at approximately 1560 cm^{-1}, which was derived from the NH_2 bending vibration of CS. The zeta potential results showed (Fig. S1†), PAA- and HA-modified SPIONs possessed a negative potential, and the Fe_3O_4@CS possessed a positive potential. The hysteresis loop (Fig. S2B†) showed no remanence or coercivity, indicating that these materials possessed super paramagnetic properties. The above results indicated that the five types of SPIONs were synthesised successfully.

The magnetic resonance imaging performance of super paramagnetic iron oxide nanoparticles is mainly affected by the size of the magnetic core[21] and the terminal functional groups.[20] As shown in Fig. S3A,† the iron oxide nanoparticles with smaller sizes exhibited better T_1 imaging performance, while the T_2 imaging effect was mostly the opposite of the T_1 imaging trend. There was a better linear relationship between the R_1/R_2 signals of these five materials and the iron concentration corresponding to Fig. S3B.†

Effect of SPIONs on RBC morphology and lysis

Red blood cells are the most abundant blood cells, comprising approximately 50% of the total blood cells. The primary function of erythrocytes is to transport oxygen and carbon dioxide. Moreover, the integrity of RBC membranes and RBC morphology are closely associated with anaemia and thrombus formation.[30] Therefore, estimating the morphological and functional changes of RBCs has been frequently used for assessing the blood compatibility of biomaterials, which also has the advantage of secure handling, high abundance, and importance.[31]

RBC lysis. Haemolysis refers to the phenomenon in which damaged erythrocyte membranes release haemoglobin from the cell, indicating a disturbance of RBC membrane integrity. This has been widely applied in blood compatibility assessment. Generally, the haemolytic properties of biomaterials are

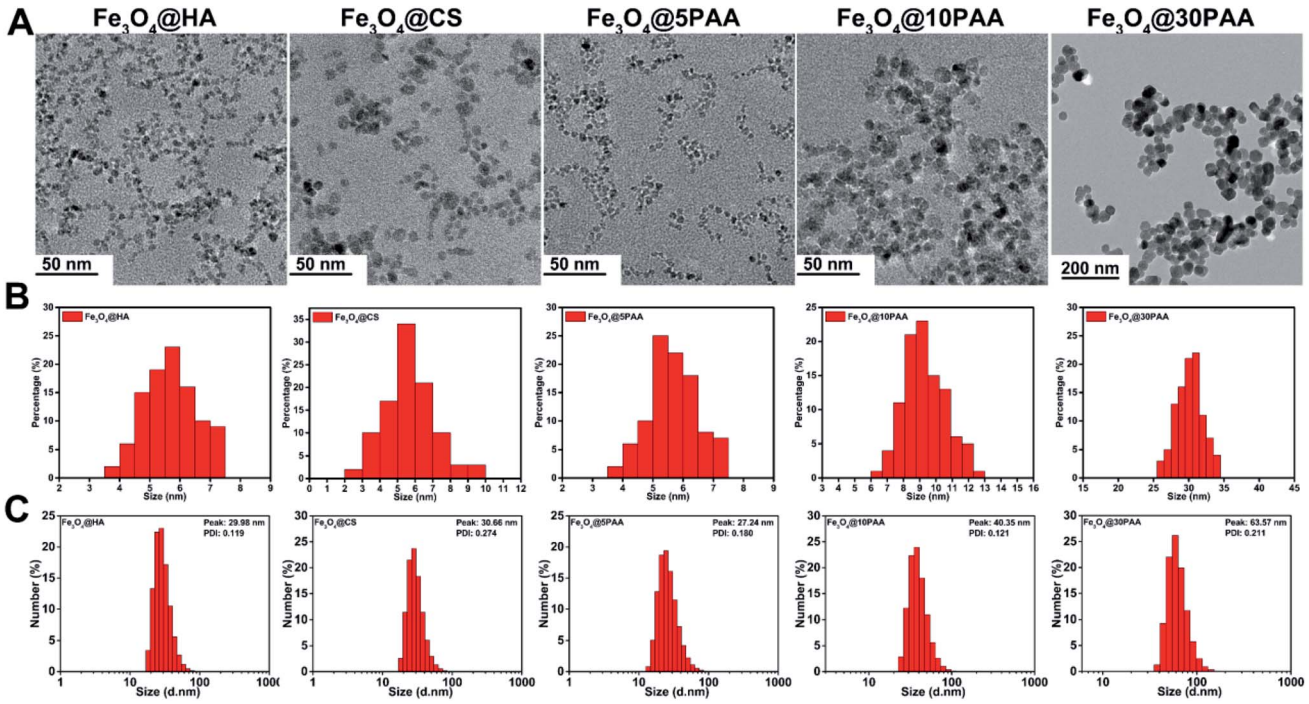

Fig. 1 The size distribution of SPIONs (A) TEM images (B) the corresponding diameter distribution of SPIONs from TEM. (C) The hydrodynamic size distribution of SPIONs.

evaluated by measuring the haemolysis rate of the material after incubating with red blood cells. If the haemolysis rate is higher than 5%, the rate is considered a positive result.

Various polymers and nanoparticle have shown different behaviors when they have a contact with RBCs. HA,[32,33] CS[34,35] and PAA[36,37] were considered as safepolymers and broadly used in the field of biomaterials that do not have the serious effect to RBCs. Compared with polymer, the interactions between nanoparticles and RBCs are not only affected by the hydrophobic and electrostatic properties,[38] but also the composition, size and shape of the nanoparticles.[39] Therefore, we selected different kinds of SPIONs to perform this study. From Fig. 2, the haemolysis rate of PAA-modified SPIONs increased following the increased size for the decreased stability (Fig. S3†), which resulted in increased lysis of RBCs. Specifically, when the concentration reached 500 μg Fe mL^{-1}, Fe_3O_4@30PAA destroyed highest number of RBCs, and the haemolysis rate was nearly the same as the positive control group, in which Triton X-100 was used. Compared with the haemolytic effect of SPIONs modified with different surface ligands of the same size, we

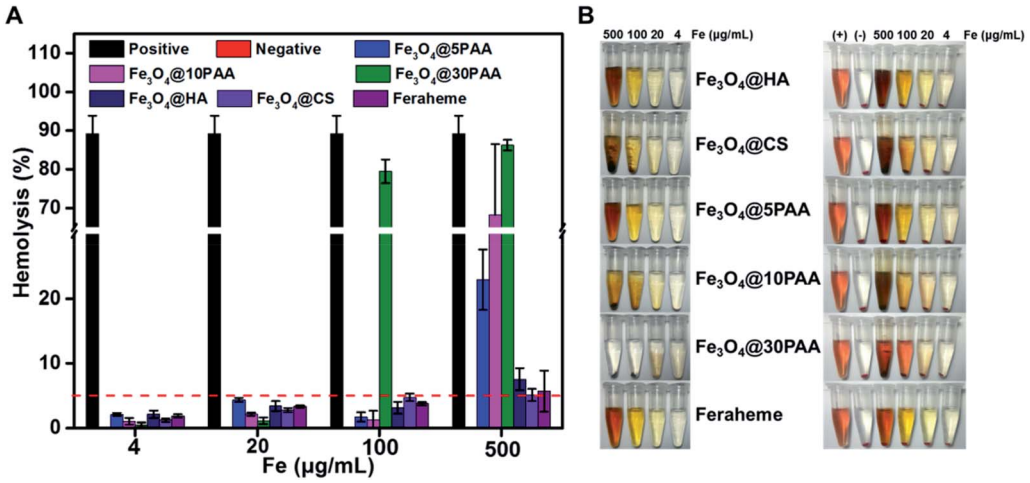

Fig. 2 Haemolytic assay of SPIONs (A) the haemolysis rate of the RBCs incubated with different concentrations of the various SPIONs. (B) Pictorial comparison of different concentrations of SPIONs with and without RBCs. The left photo shows SPIONs, while the right photo shows SPIONs and RBCs after the same treatment. Triton X-100 and PEG were used as positive and negative controls, respectively.

found that the haemolysis rate with Fe_3O_4@5PAA was 23% at 500 μg Fe mL^{-1}, which is much higher than that with Fe_3O_4@HA (7.5%), Fe_3O_4@CS (5.1%), and Feraheme (5.7%), showing that PAA might have a strong interaction with the RBC membrane. Furthermore, the increase in haemolysis rate was positively correlated with increasing concentrations of iron. All the haemolysis rates were less than 5% at 4 and 20 μg Fe mL^{-1} of SPIONs, indicating relatively safe features. Notably, the haemolysis rate of these SPIONs were more than 5% at the highest concentration (500 μg Fe mL^{-1} approximately), which is likely due to the concentration of elemental iron being 23 times higher than the imaging dose used in the clinic.[40] Our findings demonstrated that HA and CS are more suitable surface ligands on SPIONs for biomedical applications since these modified SPIONs did not lead to haemolysis at practically used concentrations. These results coincided with previous reports.[18]

RBC morphology. The shape of mature red blood cells is a biconcave disk. If the typical shape of the red blood cells is changed, their physiological function will be damaged.[41] Therefore, this work studied the effect of SPIONs of different sizes and decorated with different surface ligands on the aggregation and morphology of red blood cells.

For the three types of PAA-modified iron oxide nanoparticles of different sizes, the morphological alteration of RBCs was directly correlated with increased particle size (Fig. 3). At 500 μg Fe mL^{-1}, Fe_3O_4@5PAA had agminated some RBCs, while the Fe_3O_4@10PAA treatment produced the greatest RBC agmination and produced crenate RBC morphology. Most seriously, Fe_3O_4@30PAA caused devastating destruction of almost all RBCs and it was difficult to identify intact red blood cells in the field of view. In Fig. 3, the aggregation of Fe_3O_4@10PAA nanoparticles was found on the surfaces of red blood cells. These test results are largely consistent with the haemolysis results demonstrating that increasing size will reduce the stability of SPIONs in the physiological environment (Fig. S4†) to trigger greater destruction on erythrocyte membranes. As indicated in previous reports, the aggregated nanoparticles have a substantial effect on cell cytotoxicity,[42] and our results confirmed this point.

At the same particle size, the degree of RBCs damage was increased in the following order: Feraheme, Fe_3O_4@HA, Fe_3O_4@CS, and Fe_3O_4@5PAA, indicating the nature of polysaccharide used as a surface ligand on SPIONs was better than PAA. The surface roughness and morphological change of red blood cells could also be observed in the Fe_3O_4@CS group, while Fe_3O_4@HA caused little change of RBC Morphology compared with the Feraheme group and the PBS group at the same iron concentration. The reason for this finding might be that the interaction between positively charged Fe_3O_4@CS and the negatively charged RBC lipid layer was stronger than the Fe_3O_4@HA, whose surface charge was negative.[43] However, the severe aggregation could not be seen in the RBCs treated with Fe_3O_4@CS. A possible explanation for this finding is that Fe_3O_4@CS, with a positive charge, surrounded the RBC surfaces and prevents the severe aggregation of RBCs due to electrostatic repulsion.[44] Overall, the effect of the materials on red blood cell morphology showed a concentration-dependent relationship, and as described above, HA- and CS-modified SPIONs have relatively better biosafety compared with PAA. Furthermore, our results are also consistent with a report that Fe_3O_4-MNPs in a high iron concentration will have a risk of inducing thrombus formation.[18]

Platelet aggregation

Platelets are the smallest group of cells in human blood. Platelets are irregularly shaped, with an average diameter of approximately 2–4 μm, which plays a vital role in the promotion of haemostasis and the acceleration of blood clotting. The number of healthy human platelets is (100–300) $\times 10^9$ cells per L. An abnormally reduced number of platelets may lead to poor thrombosis and haemorrhage, and cause significant harm to the human body. Therefore, the determination of the platelet aggregation rate is an integral part of evaluating blood compatibility of biological materials and reflects the risk of thrombus formation. Collagen was used as a positive control for platelet aggregation in this experiment.

As shown in Fig. 4, the number of platelets treated with Fe_3O_4@10PAA and Fe_3O_4@5PAA were different from the negative control group. These two groups produced an aggregation of platelets, and the aggregation rates were 79.4% and 44.0%, respectively, which indicated that SPIONs with smaller sizes

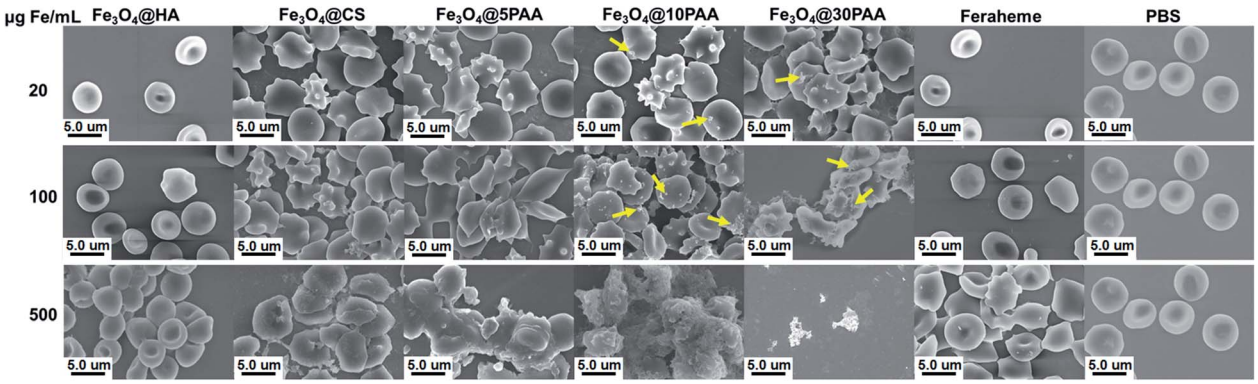

Fig. 3 SEM images of the morphology and aggregation of RBCs in the presence of SPIONs with different iron concentrations. Yellow arrows indicate aggregated nanoparticles.

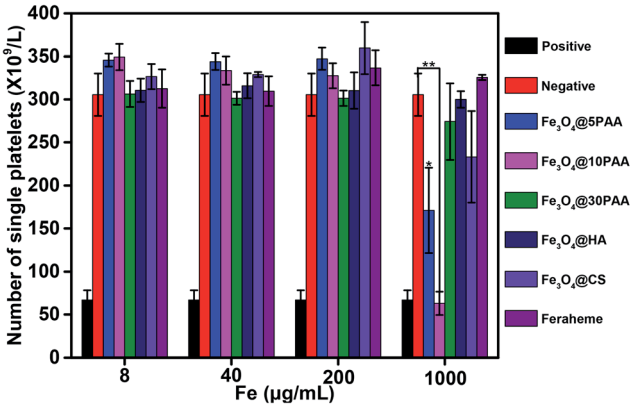

Fig. 4 The degree of platelet aggregation determined after PRPs were treated with different concentrations of SPIONs. PBS was used as a negative control, and collagen was used as a positive control. Statistical significance is assessed by Student's *t* test compared to the negative group. $p < 0.05$ (*) and $p < 0.01$ (**).

tend to induce platelet aggregation. Compared with the effect of SPIONs decorated with different ligands on platelet aggregation, SPIONs modified with PAA triggered a greater reduction of single platelet numbers. It had been reported that chitosan nanoparticles with a comparatively high surface charge (14.1 ± 0.6 mV) showed platelet compatibility,[45] which corresponded with our results showing that Fe_3O_4@CS with a higher positive charge did not induce significant platelet aggregation. In all groups, platelet numbers declined only at the highest concentration of approximately 1 mg Fe mL^{-1}. They reflected platelet activation, which was different from the result that USPION at 0.2 μg mL^{-1} caused a significant platelet aggregation effect.[17] The extent of platelet aggregation caused by SPIONs may be connected with both the surface ligand and the size of nanoparticles.

Effect of SPIONs on blood coagulation *in vitro* and *in vivo*

The effect of biological material on the coagulation system determines whether a given material can be introduced smoothly to the clinic.[14] Coagulation is divided into two pathways, endogenous coagulation, and exogenous coagulation.[46] Activated partial thromboplastin time (APTT) and prothrombin time (PT) is measured clinically to reflect the endogenous and exogenous coagulation pathways, respectively.[47] In contrast, thrombin time (TT) is an indicator of the common coagulation pathway.[48] Fibrinogen (FIB) is the precursor of fibrin and the primary substrate for the clotting process.[49] Thus, APTT, PT, TT and FIB are commonly used to employ the coagulation effect.

Fig. 5 shows that Fe_3O_4@5PAA induced the longest coagulation time (APTT and TT) than Fe_3O_4@10PAA and Fe_3O_4@30-PAA, while Fe_3O_4@30PAA mainly prolonged PT comparing with Fe_3O_4@5PAA and Fe_3O_4@10PAA. This result indicated that Fe_3O_4@5PAA inhibited endogenous coagulation. In contrast, Fe_3O_4@30PAA prolonged clotting time by inhibiting exogenous pathways of coagulation. Meanwhile, we also found that PAA-

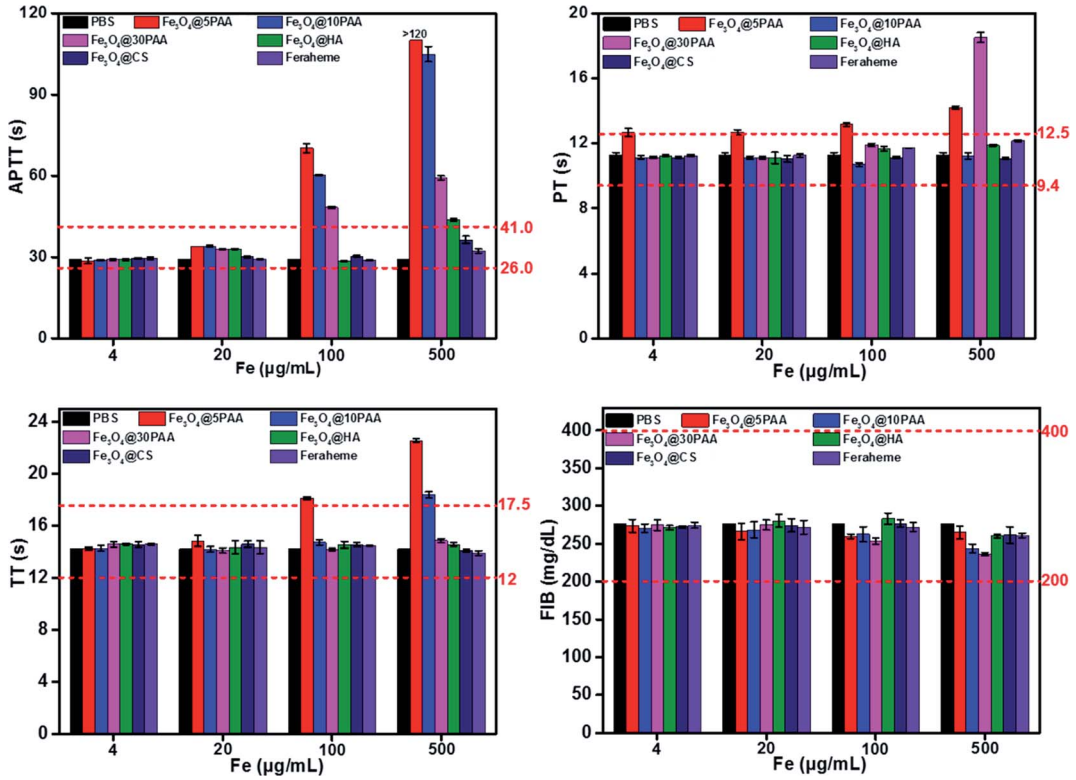

Fig. 5 The results of four coagulation tests of different concentrations of SPIONs *in vitro*. The red dotted lines represent the normal range of the coagulation parameters.

modified SPIONs significantly lengthened PT, APTT, and TT at concentrations of 100 and 500 μg Fe mL^{-1} compared with those of CS and HA. In our study, positively charged Fe_3O_4@CS merely prolonged APTT compared with the PBS control group, but the values were within a reasonable range, which showed the relative biosafety of CS. Furthermore, the clotting time in all groups was in a rational range when the concentrations were 4 and 20 μg Fe mL^{-1}, and PAA-modified SPIONs showed strong anticoagulant behaviour at higher concentrations of 100 and 500 μg Fe mL^{-1}.

Two possible reasons might explain the prolonged clotting time results.[50] One, materials caused the loss of one or several coagulation factors. For another, there were some inhibitory factors in the plasma itself. To elucidate the primary mechanism, we selected the plasma treated by the highest concentration of Fe_3O_4@PAA mixed with fresh plasma to measure clotting time again.[50] The results showed that the clotting time was significantly reduced (Fig. S5†) compared with the coagulation time measured previously. Thus, we concluded that SPIONs modified with PAA could prolong the coagulation time, given a lack of some coagulation factor.

To better explain the coagulation effects, we measured clotting time *in vivo*. A medium dose of 20 mg Fe kg^{-1} body weight[51] was administrated to BALB/c mice by tail vein injection. Blood was collected by removing the eyeball at 30 min and 24 h post-injection. Plasma was separated for the determination of coagulation. It was found that although some values were significantly different from the control group, the fluctuation range was in a rational range (Fig. 6), which was considered to have little effect on the coagulation system. The reason for different results *in vitro* and *in vivo* might be not only a long period of interaction between SPIONs and blood *in vivo* but also cellular and noncellular components of the blood. Another possible reason maybe, that the mechanisms by which the nanoparticles modulate the blood coagulation system are different in human beings and rats.[48]

Complement activation by SPIONs

Complement which is an inactive group of proteins in the serum of organism, plays an important role in enzymatic activity and belongs to the intrinsic immune system.[41] The complement system is activated mainly through three pathways: the classical pathway, the alternative pathway, and the MBL pathway. C3 plays a central role in all of the three activation pathways. C3a produced after activation is stably present in plasma, so the extent of complement activation can be reflected

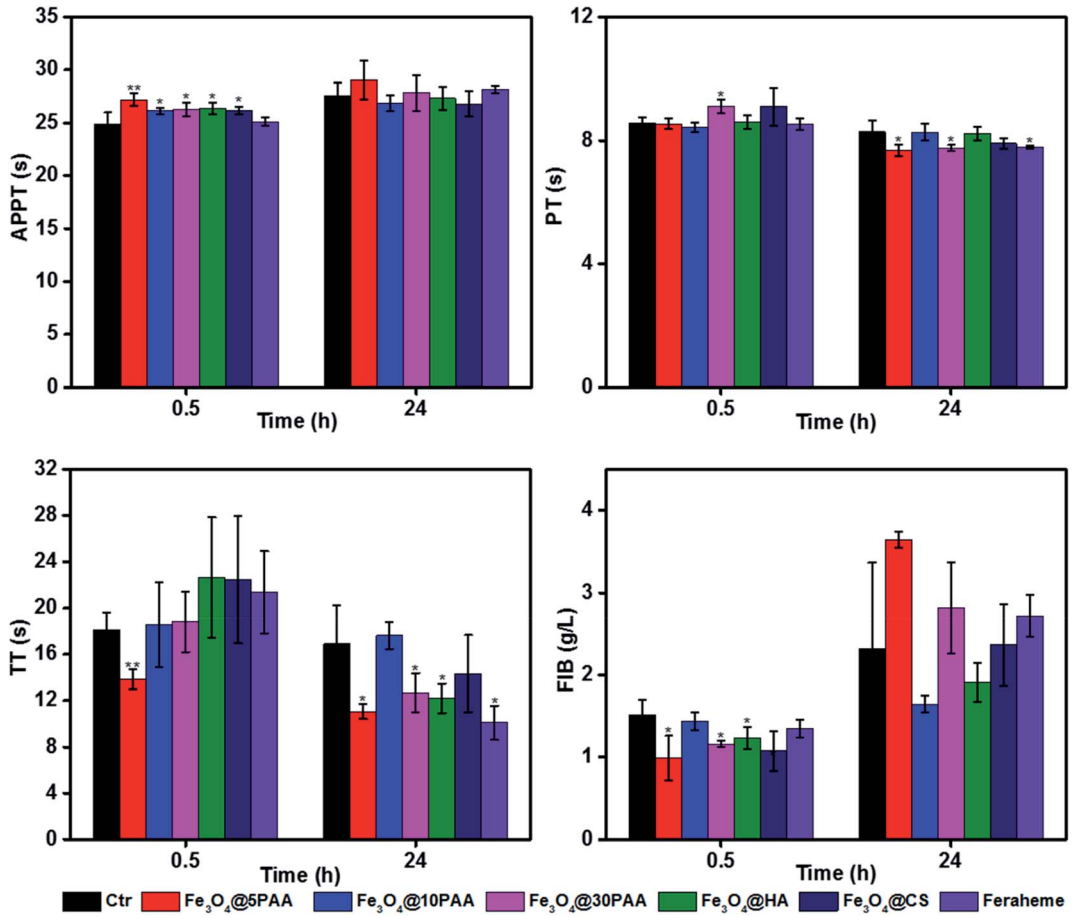

Fig. 6 Four coagulation tests measured 0.5 h and 24 h after the intravenous administration of SPIONs and saline (control) in mice. Statistical significance is assessed by Student's *t* test compared to the corresponding saline-treated group ($n = 6$). *$P < 0.05$ and **$P < 0.01$.

by the concentration of C3a in plasma.[31] The activation of complement may result in inflammation and vascular damage,[52] therefore it is an important indicator of blood compatibility.

The results (Fig. 7) showed that the increasing size of PAA-modified SPIONs augmented the degree of complement activation in the medium (0.2 mg mL^{-1}) and high (1 mg mL^{-1}) iron concentration. This finding indicates that PAA-modified SPIONs with larger sizes had strong interactions with plasma and easily activated C3. Notably, Fe_3O_4@HA also significantly activated the complement system at medium and high iron concentrations compared with Fe_3O_4@5PAA, Fe_3O_4@CS, and Feraheme, which is due to its ample –OH and –COOH groups.[53,54] In addition, as the iron concentration increased, Fe_3O_4@HA, Fe_3O_4@CS and Feraheme did not noticeably increase the degree of complement activation, while SPIONs modified with PAA enhanced the activation of complement, showing that SPIONs modified with HA and CS had better compatibility than PAA modification of the complement system.

Effect of SPIONs on HUVECs

Vascular endothelial cells form the inner wall of blood vessels, and their primary function is to phagocytose foreign matter, bacteria, necrotic cells, and aging tissues, and participate in the immune response. Endothelial impairment is a key component of multiple vascular diseases[46] and is an important aspect of blood safety assessment. Thus, human umbilical vein endothelial cells (HUVEC) were selected as the study object to determine the viability of cells after incubation with SPIONs for 24 h.

In the experiment, the supernatant was washed with PBS before adding CCK-8 reagent, and the supernatant was discarded to eliminate the influence of the absorption of the material itself. We found that these materials showed no detectable toxicity in HUVEC cells at a high concentration, up to 400 μg Fe mL^{-1}. Cell viability mostly exceeded 100% (Fig. 8), indicating the safety of SPIONs. These results were the same as a previous report that Fe_3O_4 nanoparticles are non-toxic to HUVEC[55] or even promote the proliferation of HUVEC.[56]

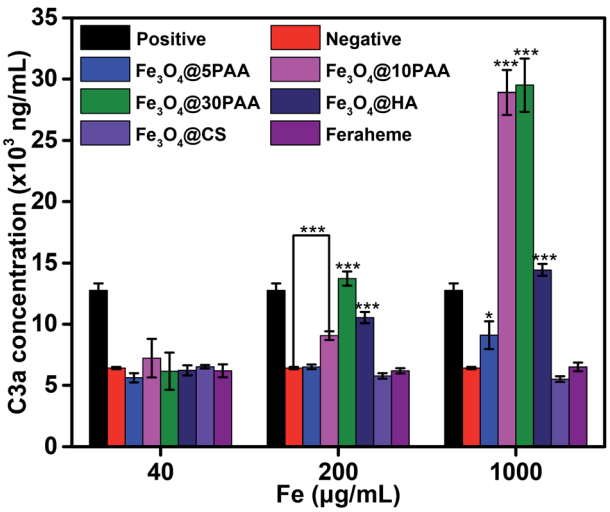

Fig. 7 *In vitro* complement system activation by different concentrations of SPIONs, with PBS as a negative control, and inulin (10 mg mL^{-1}) as a positive control; statistical significance is assessed by Student's *t* test compared with negative group. $p < 0.05$ (*), and $p < 0.001$ (***).

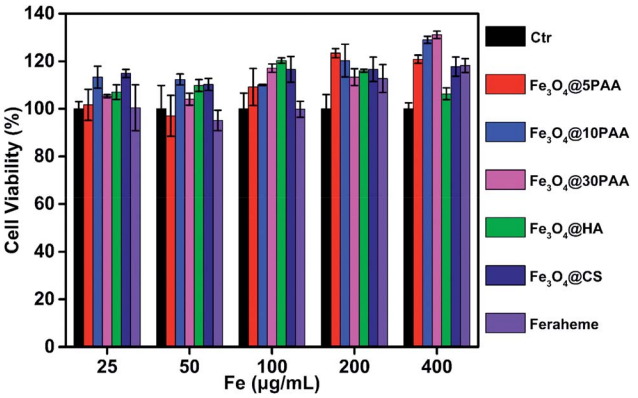

Fig. 8 Cell viability of SPIONs. The HUVECs were treated with SPIONs at different concentrations for 24 h.

Conclusion

In this study, we investigated the effects of different sizes and different surface ligands on the blood compatibility of SPIONs, including the influences on red blood cells, platelets, the coagulation system, complement activation, and vascular endothelial cells. We found smaller sized SPIONs demonstrated better stability than the larger one, and the relative larger-diameter PAA modified SPIONs were unstable under physiological conditions, aggregated quickly, and caused greater and much more severe damage to red blood cells. For different surface ligands, natural polysaccharide-(HA and CS) modified SPIONs had better blood compatibility. In contrast, organic ligand PAA-modified SPIONs caused haemolysis, abnormal morphological changes of red blood cells, aggregation of platelets, prolonged clotting time, and complement activation at relatively high concentrations. SPIONs did not show detectable toxicity to vascular endothelial cells, but a slightly proliferating effect. Notably, we also found that PAA-modified SPIONs showed greater concentration-dependence than other SPIONs for haemocompatibility. Taken together, our research will provide a reference for designing effective and safe iron oxide nanoparticles for biomedical applications.

Conflicts of interest

The authors have no conflicts of interest to declare.

Acknowledgements

This work was supported by the Ministry of Science and Technology of China (2016YFA0201600 and 2016YFE0133100), the

Science Fund for Creative Research Groups of the National Natural Science Foundation of China (11621505), the National Natural Science Foundation of China (31700879, 31900997), the CAS Key Research Program for Frontier Sciences (QYZDJ-SSW-SLH022), the CAS interdisciplinary innovation team, and the National Science Fund for Distinguished Young Scholars (11425520), the Young Elite Scientists Sponsorship Program by Chinese Society of Toxicology.

References

1 L. Zhang, W. F. Dong and H. B. Sun, *Nanoscale*, 2013, **5**, 7664–7684.
2 X. L. Zhao, H. L. Zhao, Z. Y. Chen and M. B. Lan, *J. Nanosci. Nanotechnol.*, 2014, **14**, 210–220.
3 A. Usman, U. Sadat, A. J. Patterson, T. Y. Tang, K. Varty, J. R. Boyle, M. P. Armon, P. D. Hayes, M. J. Graves and J. H. Gillard, *Nanomedicine*, 2015, **10**, 3077–3087.
4 M. Suzuki, L. Bachelet-Violette, F. Rouzet, A. Beilvert, G. Autret, M. Maire, C. Menager, L. Louedec, C. Choqueux, P. Sabboural, O. Haddad, C. Chauvierre, F. Chaubet, J. B. Michel, J. M. Serfaty and D. Letourneur, *Nanomedicine*, 2015, **10**, 73–87.
5 M. Magro, D. Baratella, E. Bonaiuto, A. R. J. de and F. Vianello, *Curr. Med. Chem.*, 2018, **25**, 540–555.
6 R. Jin, B. Lin, D. Li and H. Ai, *Curr. Opin. Pharmacol.*, 2014, **18**, 18–27.
7 S. Palanisamy and Y. M. Wang, *Dalton Trans.*, 2019, **48**, 9490–9515.
8 R. Jin, L. Liu, W. Zhu, D. Li, L. Yang, J. Duan, Z. Cai, Y. Nie, Y. Zhang, Q. Gong, B. Song, L. Wen, J. M. Anderson and H. Ai, *Biomaterials*, 2019, **203**, 23–30.
9 Y. X. Wang, *World J. Gastroenterol.*, 2015, **21**, 13400–13402.
10 S. Sharifi, S. Behzadi, S. Laurent, M. L. Forrest, P. Stroeve and M. Mahmoudi, *Chem. Soc. Rev.*, 2012, **41**, 2323–2343.
11 ISO 10993-4:2009, *Biological evaluation of medical devices. Part 4: selection of tests for interactions with blood*, 2017.
12 A. Mayer, M. Vadon, B. Rinner, A. Novak, R. Wintersteiger and E. Frohlich, *Toxicology*, 2009, **258**, 139–147.
13 E. Smyth, A. Solomon, A. Vydyanath, P. K. Luther, S. Pitchford, T. D. Tetley and M. Emerson, *Nanotoxicology*, 2015, **9**, 356–364.
14 A. N. b. Ilinskaya and M. A. Dobrovolskaia, *Nanomedicine*, 2013, **8**, 969–981.
15 S. Inturi, G. Wang, F. Chen, N. K. Banda, V. M. Holers, L. Wu, S. M. Moghimi and D. Simberg, *ACS Nano*, 2015, **9**, 10758–10768.
16 A. Soundararajan, R. J. Muralidhar, R. Dhandapani, J. Radhakrishnan, A. Manigandan, S. Kalyanasundaram, S. Sethuraman and A. Subramanian, *J. Mater. Sci.: Mater. Med.*, 2018, **29**, 145.
17 A. Nemmar, S. Beegam, P. Yuvaraju, J. Yasin, S. Tariq, S. Attoub and B. H. Ali, *Part. Fibre Toxicol.*, 2016, **13**, 22.
18 Q. Ran, Y. Xiang, Y. Liu, L. Xiang, F. Li, X. Deng, Y. Xiao, L. Chen, L. Chen and Z. Li, *Sci. Rep.*, 2015, **5**, 16209.
19 A. Ruiz, L. M. A. Ali, P. R. Caceres-Velez, R. Cornudella, M. Gutierrez, J. A. Moreno, R. Pinol, F. Palacio, M. L. Fascineli, R. B. de Azevedo, M. P. Morales and A. Millan, *Toxicol. Res.*, 2015, **4**, 1555–1564.
20 J. Zeng, L. Jing, Y. Hou, M. Jiao, R. Qiao, Q. Jia, C. Liu, F. Fang, H. Lei and M. Gao, *Adv. Mater.*, 2014, **26**, 2694–2698.
21 J. Park, E. Lee, N. M. Hwang, M. Kang, S. C. Kim, Y. Hwang, J. G. Park, H. J. Noh, J. Y. Kim, J. H. Park and T. Hyeon, *Angew. Chem., Int. Ed. Engl.*, 2005, **44**, 2873–2877.
22 V. B. Lokeshwar, D. Rubinowicz, G. L. Schroeder, E. Forgacs, J. D. Minna, N. L. Block, M. Nadji and B. L. Lokeshwar, *J. Biol. Chem.*, 2001, **276**, 11922–11932.
23 R. Mo, T. Jiang, R. DiSanto, W. Tai and Z. Gu, *Nat. Commun.*, 2014, **5**, 3364.
24 R. C. Savani, G. Y. Cao, P. M. Pooler, A. Zaman, Z. Zhou and H. M. DeLisser, *J. Biol. Chem.*, 2001, **276**, 36770–36778.
25 J. A. Burdick and G. D. Prestwich, *Adv. Mater.*, 2011, **23**, H41–H56.
26 H. Zhou, J. Tang, J. Li, W. Li, Y. Liu and C. Chen, *Nanoscale*, 2017, **9**, 3040–3050.
27 A. del Pozo-Rodriguez, S. Pujals, D. Delgado, M. A. Solinis, A. R. Gascon, E. Giralt and J. L. Pedraz, *J. Controlled Release*, 2009, **133**, 52–59.
28 D. Couto, M. Freitas, F. Carvalho and E. Fernandes, *Curr. Med. Chem.*, 2015, **22**, 1808–1828.
29 ASTM E2524-2008(2013), *Standard test method for analysis of hemolytic properties of nanoparticles*, 2013.
30 H. Kamada, Y. Imai, M. Nakamura, T. Ishikawa and T. Yamaguchi, *Med. Eng. Phys.*, 2012, **34**, 1411–1420.
31 S. Li, Z. Guo, Y. Zhang, W. Xue and Z. Liu, *ACS Appl. Mater. Interfaces*, 2015, **7**, 19153–19162.
32 H. Du, P. Liu, J. Zhu, J. Lan, Y. Li, L. Zhang, J. Zhu and J. Tao, *ACS Appl. Mater. Interfaces*, 2019, **11**, 43588–43598.
33 Y. Zhang, D. Yang, H. Chen, W. Q. Lim, F. S. Z. Phua, G. An, P. Yang and Y. Zhao, *Biomaterials*, 2018, **163**, 14–24.
34 H. H. Deng, X. L. Lin, Y. H. Liu, K. L. Li, Q. Q. Zhuang, H. P. Peng, A. L. Liu, X. H. Xia and W. Chen, *Nanoscale*, 2017, **9**, 10292–10300.
35 H. Wang, J. Qian and F. Ding, *J. Mater. Chem. B*, 2017, **5**, 6986–7007.
36 D. Li, X. Huang, Y. Wu, J. Li, W. Cheng, J. He, H. Tian and Y. Huang, *Biomater. Sci.*, 2016, **4**, 272–280.
37 C. Xu, Y. Yan, J. Tan, D. Yang, X. Jia, L. Wang, Y. Xu, S. Cao and S. Sun, *Adv. Funct. Mater.*, 2019, **29**, 8101846.
38 R. A. Jones, C. Y. Cheung, F. E. Black, J. K. Zia, P. S. Stayton, A. S. Hoffman and M. R. Wilson, *Biochem. J.*, 2003, **372**, 65–75.
39 K. M. de la Harpe, P. P. D. Kondiah, Y. E. Choonara, T. Marimuthu, L. C. du Toit and V. Pillay, *Cells*, 2019, **8**, 1209.
40 L. H. Bu, J. Xie, K. Chen, J. Huang, Z. P. Aguilar, A. Wang, K. W. Sun, M. S. Chua, S. So, Z. Cheng, H. S. Eden, B. Z. Shen and X. Y. Chen, *Contrast Media Mol. Imaging*, 2012, **7**, 363–372.
41 Y. Zhang, C. Y. Wang, R. S. Hu, Z. H. Liu and W. Xue, *ACS Biomater. Sci. Eng.*, 2015, **1**, 139–147.
42 L. Q. Chen, L. Fang, J. Ling, C. Z. Ding, B. Kang and C. Z. Huang, *Chem. Res. Toxicol.*, 2015, **28**, 501–509.
43 H. Kettiger, G. Quebatte, B. Perrone and J. Huwyler, *Biochim. Biophys. Acta*, 2016, **1858**, 2163–2170.

44 X. Liu, Y. Mo, X. Liu, R. Guo, Y. Zhang, W. Xue, Y. Zhang, C. Wang and S. Ramakrishna, *Mater. Sci. Eng., C*, 2016, **62**, 173–182.
45 X. Li, A. Radomski, O. I. Corrigan, L. Tajber, F. De Sousa Menezes, S. Endter, C. Medina and M. W. Radomski, *Nanomedicine*, 2009, **4**, 735–746.
46 D. B. Cines, E. S. Pollak, C. A. Buck, J. Loscalzo, G. A. Zimmerman, R. P. McEver, J. S. Pober, T. M. Wick, B. A. Konkle, B. S. Schwartz, E. S. Barnathan, K. R. McCrae, B. A. Hug, A. M. Schmidt and D. M. Stern, *Blood*, 1998, **91**, 3527–3561.
47 D. Zhong, Y. Jiao, Y. Zhang, W. Zhang, N. Li, Q. Zuo, Q. Wang, W. Xue and Z. Liu, *Biomaterials*, 2013, **34**, 294–305.
48 L. Song, D. Zhu, L. Liu, X. Dong, H. Zhang and X. Leng, *J. Biomed. Mater. Res., Part B*, 2010, **95**, 374–379.
49 M. M. Cushing and T. Haas, *Transfusion*, 2019, **9999**, 1–3.
50 L. M. A. Ali, M. Gutiérrez, R. Cornudella, J. A. Moreno, R. Piñol, L. Gabilondo, A. Millán and F. Palacio, *J. Biomed. Nanotechnol.*, 2013, **9**, 1272–1285.
51 L. Yang, H. Kuang, W. Zhang, Z. P. Aguilar, Y. Xiong, W. Lai, H. Xu and H. Wei, *Nanoscale*, 2015, **7**, 625–636.
52 K. N. Ekdahl, K. Fromell, C. Mohlin, Y. Teramura and B. Nilsson, *Sci. Technol. Adv. Mater.*, 2019, **20**, 688–698.
53 Y. M. Thasneem, S. Sajeesh and C. P. Sharma, *Colloids Surf., B*, 2013, **108**, 337–344.
54 K. N. Ekdahl, B. Nilsson, C. G. Golander, H. Elwing, B. Lassen and U. R. Nilsson, *J. Colloid Interface Sci.*, 1993, **158**, 121–128.
55 H. Li, Z. Lu, G. Cheng, K. F. Rong, F. X. Chen and R. Chen, *RSC Adv.*, 2015, **5**, 5059–5067.
56 Q. Y. Wu, J. Y. Shi, J. Zhang, L. Q. Zhang, Y. M. Zhao, L. Tang, Y. Chen, X. D. He, H. Liu and B. Su, *Chin. J. Oncol.*, 2013, **35**, 808–813.